Electrochimica Acta 580 (2026) 150036

Contents lists available at ScienceDirect

Electrochimica Acta

journal homepage: www.journals.elsevier.com/electrochimica-acta

# Developing an interaction model for solid polymer electrolyte/Li metal interfaces: LiTFSI-PEO as a case study

Vanessa Torres [a,b,*], Mahsa Ebadi [c], Tuanan C. Lourenço [d], Marcelo Albuquerque [d,a], Pedro Venezuela [a], Luana S. Pedroza [b], C. Moyses Araujo [e,f], Daniel Brandell [c], Luciano T. Costa [d,*]

[a] Instituto de Física, Universidade Federal Fluminense (UFF), 24210-346 Niterói, Rio de Janeiro, Brazil
[b] Instituto de Física, Universidade de São Paulo, SP 05508-090, Brazil
[c] Department of Chemistry - Ångström Laboratory, Uppsala University, Box 538, 75121 Uppsala, Sweden
[d] Instituto de Química-Molecular Modeling and Computer Simulation (MolMod-CS) Group, Universidade Federal Fluminense, Outeiro de São João Batista, s/n, Niterói 24020-141, RJ, Brazil
[e] Department of Engineering and Physics, Karlstad University, Karlstad, 651 88, Sweden
[f] Department of Physics and Astronomy, Division of Materials Theory, Uppsala University, Uppsala, Box 516, SE-75120, Sweden

ARTICLE INFO

Dataset link: https://github.com/molmodcs/Li-metal-anode-simulations

*Keywords:*
Solid polymer electrolytes
Lithium metal anodes
Molecular dynamics simulations
Force field parameterization
Interfacial ion transport

ABSTRACT

In this study, we develop a precise parameterization approach to construct an accurate classical molecular dynamics (MD) force field describing the interactions between solid polymer electrolytes (SPEs) and lithium metal anodes. Building upon our previous work (Electrochimica Acta 2017, 234, 43–51), which employed standard Lennard-Jones (LJ) interactions with cross terms obtained from conventional combination rules that resulted in significant structural ordering and slowed ionic dynamics at the explicit Li interface, we address a key limitation of that parameterization: the overestimation of short-range interfacial ordering with consequent effects on ionic dynamics. To overcome this, we performed density functional theory (DFT) calculations to parameterize the cross-term interactions, resulting in Morse potentials that describe the non-bonded interactions between the electrolyte components (poly(ethylene oxide) (PEO) and LiTFSI salt) and the metallic lithium surface. Comparative MD simulations reveal that the parametrized model based on the Morse functional form significantly modifies the interfacial structure, promoting a $[Li]^+$ and $[TFSI]^-$ rich interfacial region and increasing the participation of $[TFSI]^-$ in the $[Li]^+$ coordination environment. In addition, the parametrized Morse model reduces the artificial confinement of $[Li]^+$ ions observed with the LJ description, leading to shorter coordination lifetimes and enhanced ionic mobility. This methodological advancement offers a more reliable atomistic framework for understanding structure-dynamics relationships at lithium metal electrode interfaces and may provide a basis for future studies of other polymer-based solid-state battery systems.

## 1. Introduction

Solid electrolytes are currently considered key components in the development of safer lithium batteries with enhanced energy density [1,2]. This improvement can be partly achieved due to the reduced weight and volume of electrolyte required to operate the cell, but more significantly if the Li-metal can be used as the battery anode. However, Li-metal is generally too reactive and experiences dendrite formation when used in conventional liquid electrolytes, but solid electrolytes are expected to provide better mechanical rigidity and a stabilized surface chemistry [3].

Both ceramic and polymeric materials can be used for solid electrolytes. While solid polymer electrolytes (SPEs) possess relatively low ionic conductivity, they are likely to render significant advantages in terms of processing, cost, flexibility, and wettability when employed in Li-batteries [1]. Recent experimental studies have further emphasized the importance of the Li-metal/SPE interface [4–7]. Li et al. reported that PEO–kaolinite intercalated composites can enhance Li-ion transport and improve the interfacial stability of PEO-based electrolytes against lithium metal [5]. Similarly, Zhu et al. investigated the electrochemical behavior of lithium metal in solid polymer electrolytes,

* Corresponding authors.
*E-mail addresses:* vtorres@if.usp.br (V. Torres), ltcosta@id.uff.br (L.T. Costa).

https://doi.org/10.1016/j.electacta.2026.150036
Received 29 July 2026; Received in revised form 8 September 2026; Accepted 18 September 2026
Available online 8 October 2026
0013-4686/© 2026 The Authors. Published by Elsevier Ltd. This is an open access article under the CC BY license (http://creativecommons.org/licenses/by/4.0/).
The Article Processing Charge for the publication of this research was funded by the Coordenação de Aperfeiçoamento de Pessoal de Nível Superior - Brasil (CAPES) (ROR identifier: 00x0ma614).

emphasizing the role of current density and the progressive interfacial degradation during prolonged cycling [6]. The interfacial compatibility of SPEs with Li-metal is, however, currently poorly understood, while their solid nature limits the use of conventional experimental techniques, such as photoelectron spectroscopy [4,8]. Given the experimental challenges involved in investigating interfaces, computational modeling emerges as a powerful tool to provide atomic-level understanding of the Li-metal/electrolyte interface, an area that remains largely unexplored.

Computational studies of polymer/solid surfaces and interfaces pose several challenges, mainly due to the difficulty of considering different time and length scales simultaneously in the applied modeling techniques [9]. Within this context, there have been several studies in the literature comprising atomistic modeling of polymers interacting with solid surfaces, including determination of polymer adhesion at different surfaces or substrates using DFT calculations [10,11] or classical molecular dynamics (MD) simulations [12–14]. In general, the accuracy and usefulness of MD simulations are strictly dependent on the quality of the atomistic force field. Standard force fields such as OPLS [15] are often less suitable for soft–hard matter interfaces, since they are primarily parametrized to reproduce the properties of soft matter. Therefore, to model interactions at such interfaces, additional parameterizations or alternative types of potentials may be required. However, little attention has been devoted to the development of force fields for soft–hard matter interfaces such as polymer/solid interfaces, which currently represents a significant gap in applied computational materials science [9].

Previous computational studies of electrode/SPE interfaces have provided important insights into the interfacial structure and dynamics of polymer electrolytes.[16–20] Atomistic simulations have revealed pronounced interfacial layering and changes in $[Li]^+$ coordination at lithium-metal interfaces, leading to reduced ionic mobility in the interfacial region compared with the bulk electrolyte.[17,18] Despite these advances, accurately describing the specific interactions between PEO/LiTFSI electrolytes and metallic lithium surfaces remains a significant challenge.

In a previous study, we performed classical MD simulations of an interface between Li metal and an SPE comprising PEO and the LiTFSI (lithium bis(trifluoromethanesulfonyl)imide) salt.[21] The impact of introducing the surface on the SPE was evident from the simulations, including the formation of a double-layer-like region near the surface and a slowdown of the dynamics in the interfacial region. Although this study constituted an important first step toward modeling SPE/Li interfaces, the interaction parameters describing the electrolyte–Li metal cross terms were not specifically developed for this interface but instead obtained using conventional Lennard-Jones (LJ) combination rules. In this context, the limitation is associated with the use of generic combination rules to describe the electrolyte–Li metal cross interactions, which may not fully capture the specific characteristics of this interface, emphasizing the need for a system-specific parameterization. To obtain a more accurate description of the interactions at the interface, which are critical for battery performance, quantum mechanical calculations can provide the basis for a system-specific parameterization.

In this work, we focus on developing an improved parameterization to describe the interactions between electrolyte species and the Li-metal surface. This is achieved by performing DFT calculations on individual ions and on the PEO oligomeric unit on the Li surface, thereby obtaining force field parameters for pair interactions between electrolyte atoms and metallic Li atoms at the surface. These parameters are then employed in MD simulations of the SPE/Li-metal system. Based on the interaction profiles obtained from DFT calculations, this new parameterization is represented using a Morse potential. Among the tested functional forms, including Lennard-Jones and Buckingham potentials, the parametrized Morse potential provided the best agreement with the calculated interaction profiles for the electrolyte–Li metal cross interactions. The Morse potential has also been used to describe interactions between molecular species and metal surfaces because its functional form provides greater flexibility to reproduce the shape of surface–molecule interaction profiles [9,22,23]. In particular, compared with the Lennard-Jones form, it can provide a softer short-range repulsion and a longer-ranged attractive contribution, which may be important for accurately describing interactions at metal–molecule interfaces.

The resulting model is compared with the conventional description based on LJ cross terms obtained from generic combination rules [17,19,24]. Throughout this work, we refer to these models as the LJ and Morse descriptions for simplicity. This terminology reflects the functional form adopted for the electrolyte–Li metal cross interactions, although the principal distinction between the two approaches lies in the parameterization strategy: the previous model describes the electrolyte–Li metal cross interactions using parameters obtained from combination rules, whereas the present model employs system-specific parameters derived from DFT calculations. We analyze both parameterizations in terms of structural and dynamic properties and evaluate lithium-ion transport behavior. The resulting parameterization leads to a markedly different interfacial organization, characterized by enhanced accumulation of $[Li]^+$ and $[TFSI]^-$ near the Li-metal surface, shorter $[Li]^+$ coordination lifetimes, and modified ion transport behavior compared with the generic rule-based description. These results demonstrate that the improved description arises from the system-specific parameterization of the electrolyte–Li metal interactions rather than from the choice of the potential functional form, highlighting the importance of accurate force field development beyond standard combination rules.

## 2. Interaction model of the PEO electrolyte/Li-metal slab

Force fields are normally described by bonding and non-bonding terms, of which the bonding parts include stretching, angle bending, and torsional interactions. The non-bonded parts are van der Waals and Coulomb potentials. In this study, OPLS-AA force field parameters were used for all bonded parameters of PEO [15]. The bonded force field parameters of the $[TFSI]^-$ ion were taken from a study by Padua and Lopes [25]. These parameters are based on the OPLS-AA force field and can be integrated into it.

Three different types of interactions can be considered in the modeling of polymer electrolyte/Li-metal interfaces: (i) the interactions within the electrolyte between ions and molecules; (ii) the interaction between the electrolyte components and the Li-metal surface atoms; (iii) the interactions between the Li-metal atoms. For the first group (i), OPLS-AA force field parameters were used. To account for molecular polarization more realistically, scaled charges of 0.8e were considered for both $[Li]^+$ and $[TFSI]^-$. It has been reported that scaled-charge models in polymer electrolyte systems are essential to reproduce several structural and transport properties [18,26–30]. The interaction model for the second group (ii) was developed by identifying a suitable potential model for the interaction of the molecules/ions with the Li-metal surface from first-principles calculations. For the third group (iii), interactions among Li-metal atoms, the same LJ parameters from previous work were used [21].

In order to obtain the non-bonded parameters, a rigid potential energy scan (rPES) was carried out by gradually changing the distance between atoms in the electrolyte and Li atoms on the surface, while keeping the rest of the molecular and surface geometries fixed. This approach allows the electrolyte–surface interaction energy to be isolated as a function of distance, avoiding additional contributions arising from structural relaxation of either fragment. DFT calculations were performed using the Gaussian 16 package [31]. In order to estimate the long-range interactions of the electrolyte components and the Li surface, the M06 [32] functional was applied. Both M06-L and M06-2X [33] were checked for interactions of PEO and the Li surface for one adsorption site [the so-called top site; see Fig. 1(d)], serving as an

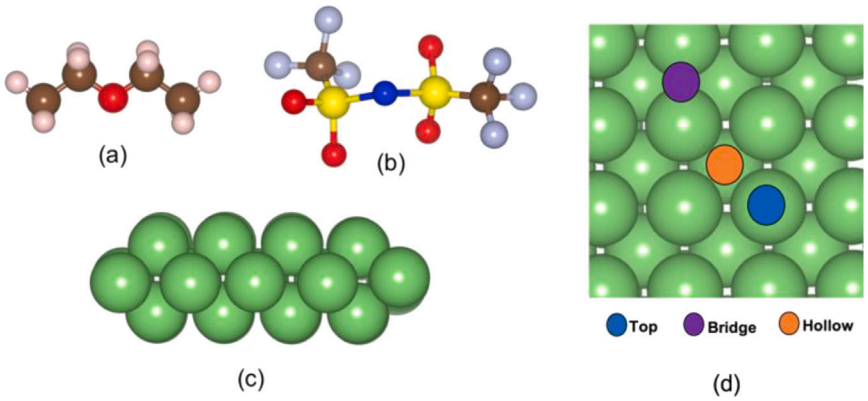


**Fig. 1.** Optimized structures of (a) diethyl ether (a model for PEO), (b) $[TFSI]^-$ and (c) the Li (100) surface. Green, red, yellow, gray, dark blue, brown and pink denote Li, O, S, F, N, C and H atoms, respectively, (d) the top, bridge and hollow sites marked with colored circles on the surface of the Li metal.

example to test the accuracy in producing the potential plot. In this test, the M06-2X functional produced better results in accordance with previous work [33]. Consequently, the M06-2X functional was used for the rest of this study for both optimization procedures and calculating rPES. Different basis sets, such as the Pople basis set (6-31G*) [34] and cc-PVDZ [35] were also tested, but the TZVP [36,37] basis set was selected due to its superior performance as a triple zeta basis set. The basis set superposition error was corrected by the counterpoise (CP) correction method [38].

Another effect that can be taken into account in the non-bonded interaction term is the induced polarization on the surface due to interactions with the electrolyte molecules; the so-called 'image charge effect'. It has been discussed in a previous MD study comprising molten alkali carbonate and metal electrodes that this effect has often been neglected due to the computational cost and complexity of using it in MD code [39]. In another MD study of olefins on an Al surface [40], on the other hand, the long range electrostatic interactions through the image charge effect were ignored because of the negligible charge on the olefin molecule. The authors argued this effect should primarily be considered if the atomic charges on the atoms are highly polar, i.e. in the order of 1e. Although image charge effects may contribute to the electrolyte–metal interaction, their explicit treatment would require the implementation of a polarizable electrode model, substantially increasing the complexity and computational cost of the simulations. Since the primary objective of the present work is to improve the short-range electrolyte–surface interactions through DFT-derived non-bonded parameters, the induced polarization of the Li-metal surface was not considered. This omission represents a limitation of the present parameterization, and the contribution of image-charge effects remains to be quantified for the Li-metal interface.

Three different potential functions were evaluated to fit the DFT results: LJ, Buckingham, and Morse potentials. The LJ and Buckingham potentials were tested together with the Morse potential during the initial comparison of the different functional forms. While the LJ and Buckingham potentials did not provide satisfactory fits to the DFT interaction profiles, the Morse potential provided the best fit and was therefore selected for the parameterization. The following equation was thereby used for the fitting of the non-bonded interactions:

$$U_{non-bonded} = D_e(\exp^{-2\alpha(r-r_e)} - 2\exp^{-\alpha(r-r_e)}) \quad (1)$$

where $D_e$, $\alpha$, and $r_e$ represent the depth of the potential, the width of the potential, and the equilibrium distance, respectively. The Morse potential has been employed in previous studies to describe non-bonded interactions [41–43]. Direct implementation of the DFT-derived potentials in the classical MD framework resulted in unphysical interfacial behavior, with ionic species such as $[Li]^+$ and $[TFSI]^-$ exhibiting a tendency to penetrate the lithium slab. Since the present force field does not explicitly account for electrode polarization, charge transfer, or chemical reactivity at the interface, the DFT-derived interaction profiles were used as a physically motivated starting point and subsequently refined within the Morse framework to obtain a stable and physically meaningful interfacial structure.

For the electrolyte-metal interaction model, the three main electrolyte components, the $[Li]^+$ cation, the $[TFSI]^-$ anion, and a $C_4H_{10}O$ molecule used as a model for the PEO repeating unit, were individually studied on the Li-metal surface. The isolated molecule of diethyl ether and $[TFSI]^-$ are shown in Figs. 1(a) and (b), respectively. A similar approach has been applied to study the interaction of ionic liquids with the surface of Fe [44].

Diethyl ether was selected as a reduced molecular model of PEO because it contains the same ether functionality present in the PEO backbone and provides a representative local chemical environment for the PEO–Li interaction. This approach allows the interaction to be investigated at the DFT level while reducing the computational cost compared with an entire PEO chain. Similarly, the Li(100) surface was represented by a three-layer slab to provide a simplified representation of the local surface environment for the interaction calculations. These reduced models were used to derive effective electrolyte-surface interaction parameters and may not fully capture the complexity of an extended PEO/Li-metal interface.

The finite surface (100) of the Li metal was built from the bulk lattice parameters of the Li metal. This surface has three layers, and the optimization process was performed by keeping the two bottom layers of the surface fixed at the Li bulk lattice parameter 3.44 Å. The Li slab was modeled symmetrically and included 57 Li atoms [see Fig. 1(c)]. The spin multiplicity (2S+1) was considered equal to 2 and 4 for the Li slab; the former value was found to be energetically more stable. The finite Li(100) model was employed to obtain the local electrolyte-Li interaction profiles required for the development of the non-bonded interaction parameters. Therefore, these DFT calculations were not intended to reproduce the full electronic structure or long-range periodic behavior of an extended Li(100) surface. The use of a finite model represents a limitation of the present parameterization, since effects associated with an extended periodic metallic surface, including long-range electronic response and periodicity, are not explicitly captured.

Three different adsorption sites – hollow, top, and bridge [see Fig. 1(d)] – were also selected for the adsorption of Li ions on the Li (100) surface. An optimization process was performed for each case to determine the most favorable adsorption site. In this case, the atoms on the Li surface were fixed during the optimization to avoid convergence problems and save computational costs. The results showed that the hollow site is the most stable site for the Li ion on the surface of Li metal, and the Li ions that were initially located on top or bridge sites moved to the adjacent hollow sites during the optimization process.

This is in agreement with other computational studies on the adsorption of a Li adatom on the surface of Li metal [45].

rPES calculations were carried out for the Li ion at the hollow site of the Li surface, as shown in Figure S1. The resulting rPES exhibits a relatively broad attractive well, approximately 2.5 Å wide, compared with the curves shown in Figures 2, S2, and S3. In addition, the short-range repulsion (r < 1.0 Å) is significantly weaker than that obtained for the other adsorption sites. These characteristics pose direct challenges for the parameterization of the non-bonded interaction because, at the hollow site, the Li ion interacts simultaneously with four surface Li atoms. Consequently, the resulting rPES reflects a collective multi-atom interaction rather than a direct Li–Li pair interaction, making it unsuitable as a reference for parameterizing a transferable pairwise non-bonded potential. Therefore, to obtain transferable pairwise non-bonded parameters, we chose the top adsorption site (the second most stable adsorption configuration) to perform the rPES shown in Fig. 2(a).

The interaction of $[TFSI]^-$ at different positions on the Li surface was determined by considering the central *N* atom on top, bridge, and hollow sites. The top site was found to be the most stable position after geometry optimization. Figure S2 shows the rPES for the interaction between TFSI and the Li surface. The adsorption energy at the top site is significantly lower than that of the bridge and hollow sites. The same approach was applied for the interaction of PEO with the Li metal surface. Figure S3 shows the results when scanning the distance between the O atom of PEO at the different adsorption sites. The top site is clearly a favorable position for the adsorption of PEO with respect to its O atom.

In the next step, rPES were fitted to the Morse potential form for all components of the electrolyte on the surface of the Li metal, as shown in Fig. 2. The nonlinear least-squares Marquardt–Levenberg algorithm was used for the fitting of the DFT results (red lines). In some cases, an empirical modification (EF) of the original rPES curves was required to better capture the expected behavior of the interaction with the Li metal surface. The rPES of the Li ion and the empirical potential (orange line) are shown in Fig. 2(a). In order to extract the complete set of parameters for non-bonding interactions of $[TFSI]^-$ with the surface, all atom types in the anion were studied: O, S, N, F, and C. For all of these atom types, only their adsorption at the top site of the surface was studied. This choice is consistent with the optimized adsorption geometry, in which the highly polar atoms in the anion (O and F) are also positioned above top sites of the surface, as can be visually confirmed in Fig. 2(e–f). Also, preliminary attempts showed significant structural rearrangement of TFSI. The results of the $[TFSI]^-$ analysis are presented in Fig. 2 (e–i), where both the empirical modification (orange line) and the fitted function (red line) are shown. The results of the simulations using the FF curves (red lines in Fig. 2) for $[TFSI]^-$ presented non-physical results, as the anions infiltrate the Li metal in the interface region, which is neither computationally feasible [46] nor experimentally reasonable [47,48]. After empirically adjusting the curve (orange lines), we obtained the parameters used in the results we present here (refer to Table S1). $C_{alkyl}$ ($CH_3$), $C_{ether}$ ($CH_2$), and $O_{PEO}$ were considered for the PEO rPES scan. The H atoms were not treated explicitly for interactions with the Li metal. Therefore, united atom models of $–CH_2–$ and $–CH_3$ were used for interactions between PEO and the Li metal, but an all-atom model was still applied for all components in the electrolyte. The rPES results of the atom types of PEO adsorbed on the surface and the fitted potentials are presented in Figs. 2(b), (c), and (d), while the obtained parameters for different atom pairs are reported in Table S1.

## 3. Molecular dynamics simulation

All MD simulations were carried out using GROMACS version 2019.6 [49,50]. First, a simulation containing only the bulk electrolyte was performed in order to obtain accurate density and volume. The initial configurations were built randomly using the PACKMOL package [51] into a cubic box containing 16 PEO chains, each with 25 EO units, 50 $[Li]^+$ cations and 50 $[TFSI]^-$ anions, i.e., for a $Li:O_{ether}$ ratio of 1:8. Thereafter, a structural minimization and equilibration for 5 ns via an annealing from 700 K to 400 K in the isothermal–isobaric (NpT) ensemble with 1 bar pressure were performed. Once 400 K was reached, the simulation was extended for another 20 ns to ensure proper density equilibration. The V-rescale [52] and Berendsen approaches were used to control temperature and pressure with coupling times of 0.1 and 1.0 ps, respectively. The leap-frog algorithm was used to integrate the equations of motion, with a time step of 2 fs. The particle mesh Ewald (PME) method [53] was used to treat electrostatic and long-range pair interactions. The real space Coulombic and van der Waals interactions were calculated using a cut-off distance of 1.2 nm.

After the bulk electrolyte simulation was finished, a bcc lithium metal slab with 810 atoms was added to the box (Fig. 3). Since periodic boundary conditions were applied in all three dimensions, vacuum regions were introduced on both sides of the slab along the *z*-axis to avoid artificial interactions between periodic images of the interface. This resulted in a rectangular parallelepiped simulation box with dimensions $L_x = L_y = 3.1$ nm and $L_z = 14$ nm. To ensure proper interaction between the surface and the electrolyte in the Morse potential model, an annealing process was required, from 700 K to 400 K in the canonical ensemble (NVT) over 5 ns. For both the Morse and LJ potential models, the system was equilibrated for 20 ns in NVT, followed by a 200 ns production run at 400 K.

In order to evaluate the effect of the new parameterization on the interactions between the electrolyte and the lithium metal slab, two sets of simulations were carried out: one in which the interactions between the electrolyte components and the Li metal atoms at the surface were described by LJ cross interactions obtained from standard geometric combination rules, and another in which these cross interactions were represented by the parametrized Morse potential described above. Throughout the remainder of this work, these two models are referred to as the LJ and Morse models, respectively, although the primary distinction between them lies in the parameterization strategy rather than in the functional form of the potential itself.

In MD simulations of ionic liquids, the atomic charges used in the force fields are derived from quantum calculations using vacuum-isolated ions. However, when using classical MD non-polarizable simulations, these charges generally result in an overestimation of ion pairing and ionic correlations, leading to slower dynamics, overestimated clustering and thereby large deviations from the experimental data in transport property calculations. This overestimation is due to the lack of charge transfer effects in the condensed phase [54–56]. For this reason, the charge scaling introduced in the previous section was adopted throughout the simulations. This widely used approach partially accounts for condensed-phase polarization effects and charge fluctuations in non-polarizable force fields [29,55,56]. Maginn and coworkers [57] applied a similar scaling approach to the LJ parameters $\sigma$, $\epsilon$ in the GAFF force field for the glyme structures, G1, G2, and G4. Through a systematic study of different scaling factors, the authors found that the use of $f^\sigma = 1.03$ and $f^\epsilon = 0.9$ was able to improve the results for different thermodynamic properties such as molar enthalpy of vaporization, viscosity, and the diffusion coefficients in comparison to the experimental data. Therefore, although the Morse potential parameters were initially derived from DFT calculations, further refinement may be required to account for condensed-phase effects not fully captured in non-polarizable MD simulations, which can lead to an overestimation of interaction strengths.

To evaluate the structural and dynamical effects of the parametrized Morse potential relative to the standard LJ model, several structural and transport properties were analyzed from the production trajectories. Structural organization at the interface and in the bulk-like region was characterized using one and two dimensional density distributions, radial distribution functions, coordination numbers, and

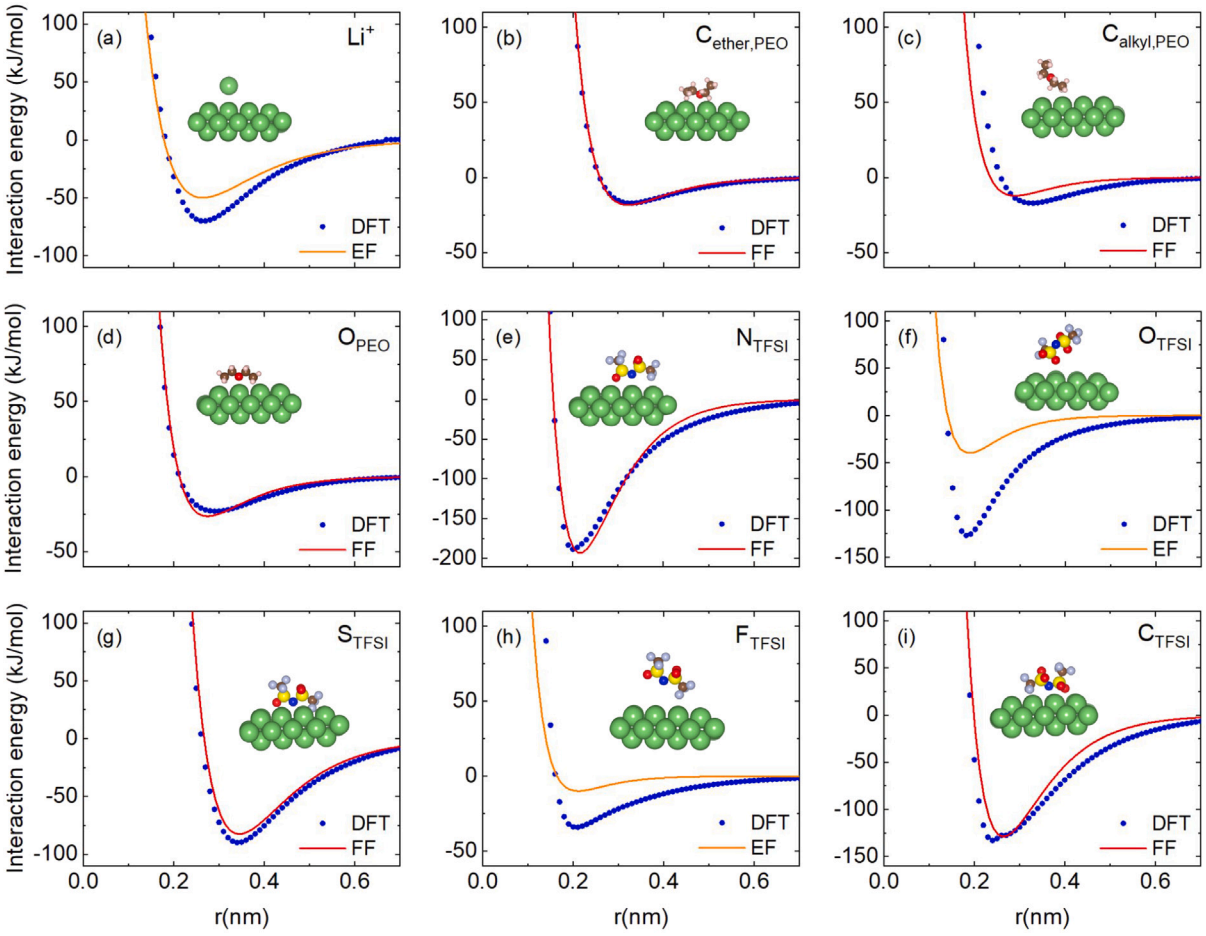


**Fig. 2.** Interaction energies of (a) $[Li]^+$ ion (b) $C_{ether,PEO}$, (c) $C_{alkyl,PEO}$, (d) $O_{PEO}$, (e) $N_{TFSI}$, (f) $O_{TFSI}$, (g) $S_{TFSI}$, (h) $F_{TFSI}$ and (i) $C_{TFSI}$ at top site at different distances from Li metal surface with CP correction, fitted function (FF) and empirical fitting (EF) to the Morse potential form.

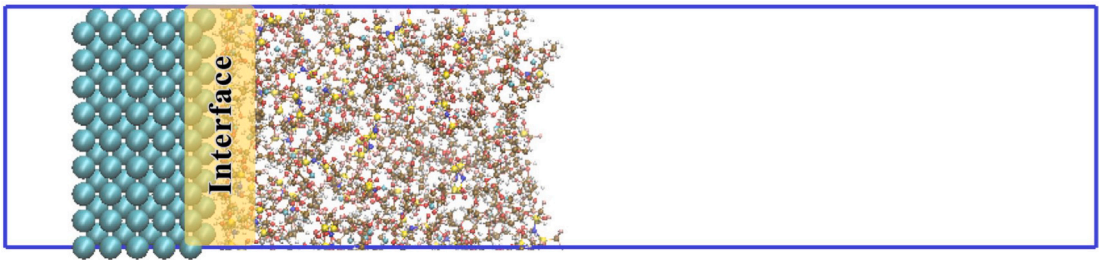


**Fig. 3.** Snapshot of the initial simulation box composed of the interface between polymer electrolyte and the metal slab.

coordination population analyses. Transport properties were investigated through mean square displacements, self-diffusion coefficients, van Hove correlation functions, and coordination time correlation functions. Finally, lithium transport mechanisms were statistically classified into continuous, vehicular, and hopping contributions.

## 4. Results and discussion

### 4.1. Structural properties

The effects of the interaction potentials describing the electrolyte–lithium metal slab were analyzed in terms of the partial density distributions for the different species along the *z*-axis. Figs. 4(a) and (b) show the partial density distributions of $[TFSI]^-$, $[Li]^+$, and PEO, obtained using either parametrized-generated potentials (Morse form) or potentials obtained from geometric combination rules (Lennard-Jones form). In both systems, the densities of the species are significantly higher near the interface, suggesting aggregation at the interface. However, the nature of the distributions differs between the two potential models. For the combination-rule potential, a 'double-layer'-like structure is observed, with primary aggregation of PEO and $[TFSI]^-$ at the interface. In contrast, the parametrized-generated potential leads to an interfacial region dominated by the two ionic species, $[Li]^+$ and $[TFSI]^-$. These differences are illustrated more clearly in Figs. 4 (c–e), which provide individual density profiles for $[Li]^+$, $[TFSI]^-$, and PEO. The findings in Fig. 4(a) agree well with previous work, where full ionic charges were used in the force field [21]. Moreover, the number density distributions seen for the parametrized-generated potentials correlate with the interaction energies shown in Fig. 2. The $[TFSI]^-$ and the $[Li]^+$ ions show stronger interaction energies with the metal slab than the PEO fragments, leading to an aggregation of the ions and resulting in a secondary distribution of the PEO in the region close to the surface.

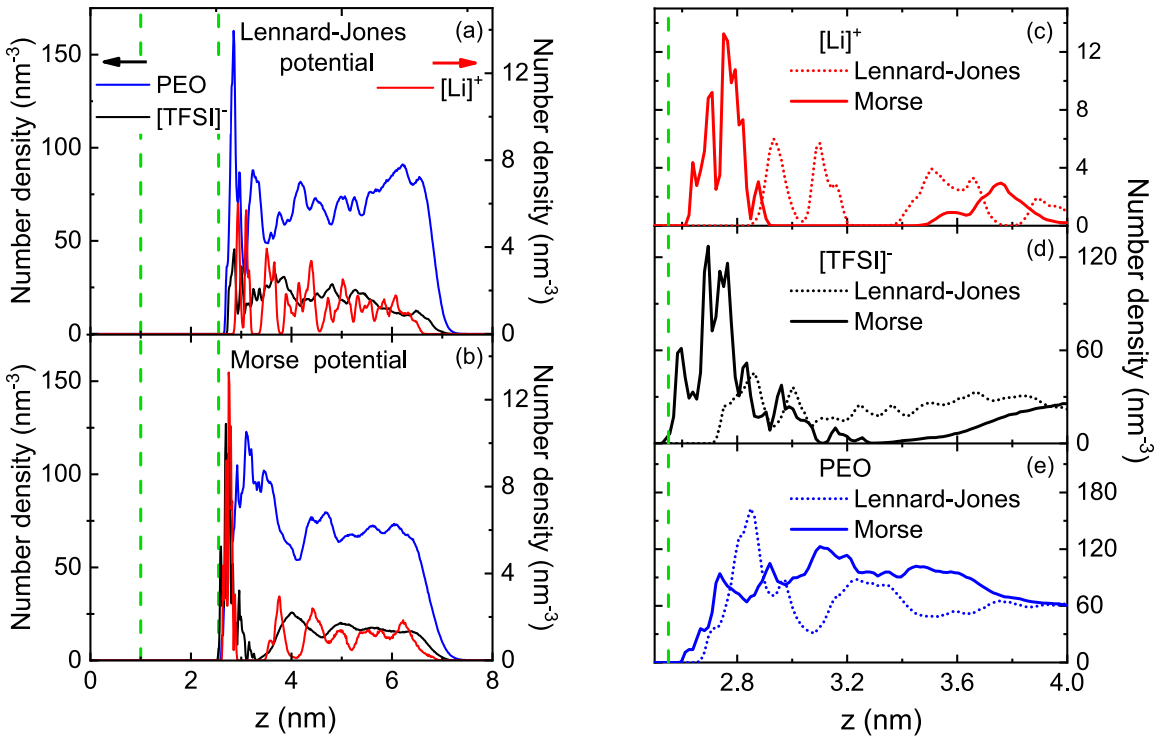


**Fig. 4.** Number density profiles of $[Li]^+$, $[TFSI]^-$, and PEO along the *z*-axis for simulations using the Lennard-Jones potential (a) and the Morse potential (b). Comparison of the density profiles for both potentials for each species: $[Li]^+$ (c), $[TFSI]^-$ (d), and PEO (e). Vertical green dashed lines denote the position of the lithium metal slab in the simulation box.

In systems comprising lithium metal anodes, dendritic lithium growth during Li deposition is a well-known issue that compromises battery performance and safety [58]. In these systems, the high reactivity of the lithium surface toward electrolyte species strongly influences the formation and composition of the Solid Electrolyte Interphase (SEI) [7,59,60]. For PEO:LiTFSI electrolytes in contact with lithium metal, it has been shown that both the polymer matrix and the $[TFSI]^-$ anion participate in interfacial degradation processes, where lithium deposition induces the formation of a lithium-rich interface accompanied by electrolyte decomposition and the generation of inorganic SEI components such as LiF, $Li_2O$, and $Li_2S$. Weintraut et al. [60], using in situ XPS and Hybrid-SIMS, revealed a spatially heterogeneous interphase at the lithium metal–polymer electrolyte interface. In this structure, inorganic species such as $Li_2O$ and $Li_2S$ are mainly found near the lithium metal, while LiF, sulfur-oxygen compounds, and degraded polymer fragments are located closer to the polymer electrolyte. However, this layering is not fixed. Some species (like $Li_2O$ and LiOH) can move within the polymer, and interphase components can migrate depending on the reaction stage. As a result, the interphase is dynamic and continuously evolves over time due to formation, dissolution, and diffusion processes.

The interfacial density distributions obtained with the parametrized Morse potential suggest that this model may provide a more consistent description of the electrolyte–metal interface than the standard LJ combination-rule approach. In particular, the preferential accumulation of $[Li]^+$ and $[TFSI]^-$ near the lithium surface is qualitatively consistent with experimental observations indicating the strong participation of ionic species in interfacial degradation and SEI formation processes [59, 60]. Although the present simulations do not explicitly account for electrode polarization, charge transfer, electrochemical reactions, or SEI formation, the enhanced accumulation of ionic species predicted by the Morse parameterization may influence the initial conditions from which these interfacial processes develop. In contrast, the LJ model predicts a comparatively stronger accumulation of polymer species at the interface.

The two-dimensional density maps of $[Li]^+$ (Fig. 5) reveal that the choice of interaction model significantly modifies the interfacial organization of the electrolyte. In the Morse description [ Figs. 5(c) and (d)], the enhanced accumulation of $[Li]^+$ near the lithium surface suggests a stronger coupling between the cation distribution and the electrode, promoting the formation of a more compact interfacial layer. In contrast, the distributions observed in the LJ model [ Figs. 5(a) and (b)] indicate that $[Li]^+$ remains more strongly influenced by coordination effects within the surrounding PEO/$[TFSI]^-$ solvation environment rather than by direct interaction with the surface. Therefore, the Morse potential leads to a distinct interfacial organization, where the relative contribution of metal–cation interactions and electrolyte solvation is altered, resulting in a modified local arrangement of $[Li]^+$ at the electrode/electrolyte interface. Overall, the differences highlight how the choice of interaction potential can significantly affect the predicted interfacial structure at the lithium metal surface. Regarding the bulk-like region, the density maps of $[Li]^+$ shown in Fig. 5 also reveal distinct behaviors. Under the LJ model, the bulk-like region exhibits a highly heterogeneous distribution, with localized high-density regions. This suggests a stronger $[Li]^+$–PEO correlation in the LJ model, where cations are more likely to be found within coordination environments associated with the polymer matrix. In contrast, the parametrized Morse potential yields a more continuous and homogeneous distribution throughout the bulk-like region.

For completeness, additional analyses including two-dimensional density maps of the oxygen atoms of PEO and $[TFSI]^-$ are provided in the Supplementary Material (Figures S4 and S5). In both interaction potentials, a similar distribution is observed throughout most of the simulation box. The main difference appears in the region close to the lithium metal surface, where, in the case of the parametrized Morse potential, both the $[TFSI]^-$ anions and the PEO chains exhibit a closer proximity to the metallic interface.

Fig. 6 shows the partial radial distribution functions (RDFs), g(r), characterizing the local interactions between $[Li]^+$ ions and the oxygen atoms of PEO and $[TFSI]^-$, both at the interface and in the bulk-like

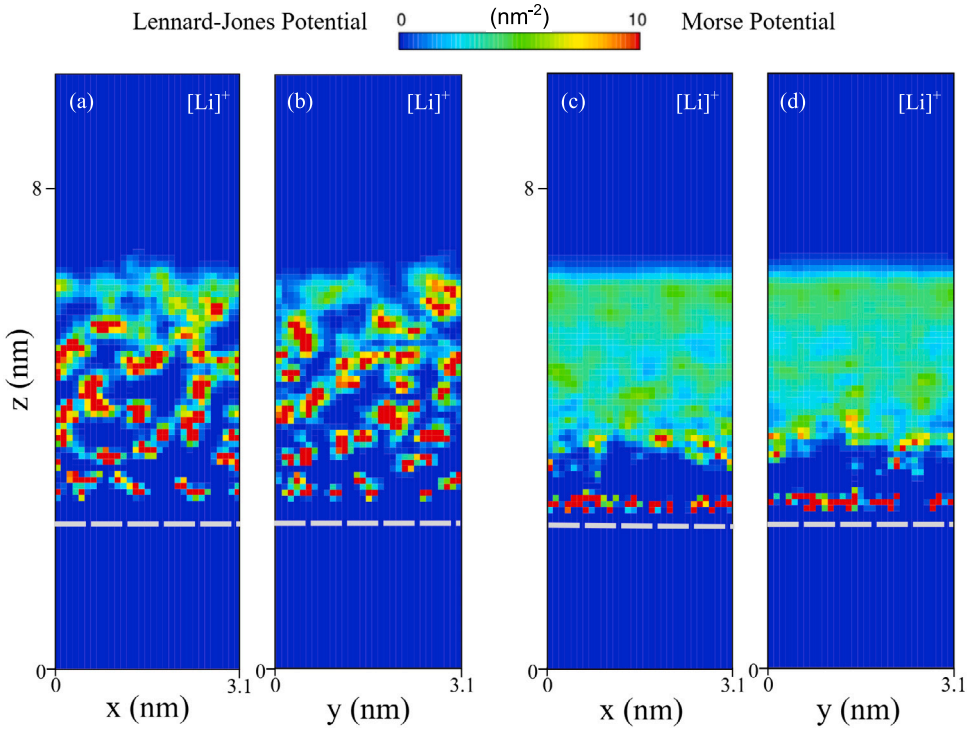


**Fig. 5.** Density maps of $[Li]^+$ in the simulation box, obtained using Lennard-Jones (a)–(b) and parametrized Morse (c)–(d) interaction potentials. The dashed gray line indicates the lithium metal surface.

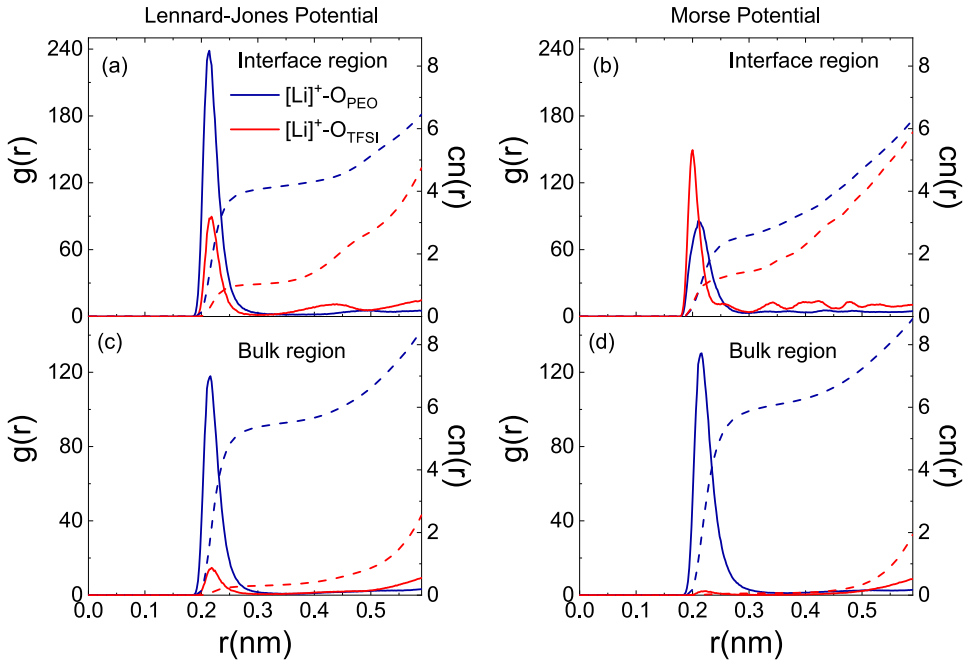


**Fig. 6.** Partial radial distribution functions, g(r) (solid lines), and accumulated coordination numbers, cn(r) (dashed lines), for the $[Li]^+$–$O_{PEO}$ and $[Li]^+$–$O_{TFSI}$ interactions in panels (a) and (b) for the interface region, and in panels (c) and (d) for the bulk-like region, using simulations with the Lennard-Jones combination rules and the parametrized Morse potential.

region, for the two potential models. These regions are defined along the z-axis: the interfacial region extends from 2.0 nm to 4.0 nm, while the remaining region is considered the bulk-like region. The definition of the interfacial region was based on the number density profiles shown in Fig. 4, which indicate that the influence of the lithium metal surface extends up to approximately 4.0 nm. This bulk-like region may still be affected by the Li-metal surface and is therefore not considered a fully independent bulk region.

For the $[Li]^+$–$O_{PEO}$ interactions in the bulk-like region [ Fig. 6(c) and (d)], both the LJ/combination rules and the Morse/parametrized potentials yield sharp and intense peaks in the g(r) functions, centered at approximately 0.22 nm. In both cases, the $[Li]^+$–$O_{PEO}$ interaction shows a significantly higher and narrower peak compared to

the $[Li]^+$–$O_{TFSI}$ interaction, indicating a stronger and more defined coordination of $[Li]^+$ with the oxygens of PEO in the bulk-like region. In contrast, the $[Li]^+$–$O_{TFSI}$ interaction shows a marked dependence on the interaction model. The Morse/parametrized potential produces a broader and less intense peak, whereas the LJ/combination rules potential results in a sharper and more intense feature. This indicates a stronger and more localized $[Li]^+$–$[TFSI]^-$ coordination in the bulk phase when using the LJ potential.

At the interfaces [ Fig. 6(a) and (b)], notable differences emerge between the two models. For the $[Li]^+$-$O_{PEO}$ interaction, both force fields display a primary peak around 0.21 nm, but the LJ/combination rules potential yields a noticeably higher intensity. In contrast, for the $[Li]^+$-$O_{TFSI}$ interaction, the Morse/parametrized potential exhibits a more intense peak centered at approximately 0.20 nm, compared to the peak around 0.22 nm observed in the LJ model. These differences reflect a key structural rearrangement at the interface. While the LJ/combination rules simulations show an overall increase in both g(r) peaks relative to the bulk-like region, in agreement with previous studies using similar force fields [34], the Morse model presents a contrasting behavior. In the Morse/parametrized potential, the $[Li]^+$-$O_{TFSI}$ peak in the interfacial region increases in intensity compared to the bulk-like region, whereas the $[Li]^+$-$O_{PEO}$ peak decreases. This is attributed to the much higher local concentration of $[TFSI]^-$ near the metal surface (as indicated by the closer peaks for the anion in Fig. 4), which leads to a partial replacement of PEO by $[TFSI]^-$ in the $[Li]^+$ solvation shell. Overall, these results indicate that the nature of the ion–metal interaction described by the force field has a direct impact on the local ion–ion coordination structure at the interface. The use of the parametrized Morse potential therefore changes not only the partial density distribution of the ions, but also the interactions between all species close to the metal slab.

We also analyzed the coordination number, cn(r), as shown in Fig. 6. In the bulk-like region [ Figs. 6(c) and (d)], $[Li]^+$ remains predominantly coordinated by ether oxygen atoms from PEO in both the LJ and Morse models, with only minor contributions from $[TFSI]^-$. In both models, $[Li]^+$ is coordinated by approximately six PEO oxygen atoms in its first coordination shell.

At the interface [ Figs. 6(a) and (b)], the LJ/combination rules model shows a slight decrease in $[Li]^+$–$O_{PEO}$ coordination to about 4.1, accompanied by an increase in $[Li]^+$–$O_{TFSI}$ coordination to approximately 1.0. In contrast, the Morse model exhibits a markedly different behavior at the interface. $[Li]^+$–$O_{TFSI}$ interactions increase significantly compared to the bulk-like region, reaching approximately 1.3, while coordination with $O_{PEO}$ decreases notably to about 2.5. Although PEO remains the primary coordinating species, these results indicate a substantial restructuring of the $[Li]^+$ coordination environment near the metal surface, with an increased participation of $[TFSI]^-$ in the $[Li]^+$ solvation shell. This effect is more pronounced in the Morse model, suggesting enhanced $[TFSI]^-$ contribution to the solvation shell at the interface in this case.

Different studies have shown that an elevated concentration of $[TFSI]^-$ anions around $[Li]^+$ is associated with the formation of $[Li]^+$–$[TFSI]^-$ ion pairs and ionic aggregates, leading to modifications in the local coordination environment and ionic transport properties [61–63]. In particular, Fortuin et al. [61] demonstrated that the ionic structure and transport properties in PEO/LiTFSI systems strongly depend on the LiTFSI concentration, leading to distinct lithium transport mechanisms in diluted and highly concentrated regimes. Complementarily, Gudla et al. [62] showed that the impact of ion pairing on ion transport is strongly related to the ion-pair dynamics and lifetime, with longer-lived ion pairs contributing negatively to ionic conductivity. In this context, the enhanced $[TFSI]^-$ concentration at the interface observed in our simulations, particularly in the Morse model, highlights the importance of further analyzing the local coordination environment of $[Li]^+$ near the metallic surface.

**Table 1**
Self-diffusion coefficients $D_i$ for $[Li]^+$, $[TFSI]^-$ and PEO in the Lennard-Jones/combination-rule and Morse potential simulations in the interface and bulk-like region (unit: $10^{-7}$ $cm^2/s$).

| Model potential | | $[Li]^+$ | $[TFSI]^-$ | PEO |
|---|---|---|---|---|
| Lennard-Jones | Interface | 0.0302 | 0.0809 | 0.0517 |
| Morse | Interface | 0.6060 | 2.9500 | 0.9580 |
| Lennard-Jones | Bulk-like region | 0.265 | 0.627 | 0.588 |
| Morse | Bulk-like region | 6.750 | 23.00 | 5.910 |

To better understand the coordination environment of $[Li]^+$ at the interface, we quantified the relative populations of $[Li]^+$ coordinated by PEO, $[TFSI]^-$, and mixed PEO–$[TFSI]^-$ environments by averaging over a 200 ns simulation (Fig. 7). In both models, the bulk-like region is dominated by $[Li]^+$ coordination with PEO, reaching 81% for the LJ potential [ Fig. 7(a)] and 96% for the Morse potential [ Fig. 7(b)]. For comparison, the same analysis was also performed considering the full system (FS). In both models, $[Li]^+$ coordination remains predominantly associated with PEO, although a noticeable contribution from mixed PEO–$[TFSI]^-$ coordination is also observed. In contrast, the interfacial region exhibits a markedly different behavior. For the LJ/combination rules potential, 55.6% of $[Li]^+$ ions remain exclusively coordinated by PEO, whereas this fraction decreases to 35% in the Morse/parametrized model, accompanied by a substantial increase in mixed PEO–$[TFSI]^-$ coordination, which reaches 51%. These results reveal a significant restructuring of the $[Li]^+$ coordination environment at the metallic interface, particularly for the Morse potential, where the increased participation of $[TFSI]^-$ anions suggests a stronger cation–anion coupling near the surface.

### 4.2. Dynamical properties

The dynamics of the particles were investigated in terms of the mean square displacement (MSD) for both potential interaction models in bulk-like and interface regions. The MSDs were calculated by the Einstein relation:

$$MSD = \langle |\vec{r}_i(t) - \vec{r}_i(0)|^2 \rangle \quad (2)$$

while the diffusion coefficients were calculated from the linear regions of the MSD using the following equation:

$$D = \frac{1}{6} \lim_{t \to \infty} \frac{d}{dt} MSD \quad (3)$$

The diffusive regime was analyzed through the $\beta(t)$ function, obtained from the local slope of the MSD; values of $\beta(t)$ near 1 correspond to normal diffusion. Table 1 shows the self-diffusion coefficients of the species in both the bulk-like and interface regions for each potential model, while the corresponding MSDs are presented in Figure S6 of the Supporting Information. For both the combination rules and the parametrized-generated potentials, the self-diffusion coefficients at the interface follow the trend $[TFSI]^-$ > PEO > $[Li]^+$. In the bulk-like region, the LJ/combination rules model shows the order $[TFSI]^-$ > PEO > $[Li]^+$, whereas the parametrized-generated potential exhibits a slightly different trend, $[TFSI]^-$ > $[Li]^+$ > PEO. The trends observed in the dynamic properties using the LJ combination rule potential are consistent with those obtained in our previous work employing a similar force field [21]. The self-diffusion coefficients in Table 1 reveal that the parametrized Morse potential leads to significantly higher mobility for all species compared to the LJ/combination rules model, in both the interface and bulk-like regions. In general, the self-diffusion results indicate that strong interactions between the lithium metal surface and the species lead to a reduction in their mobility at the interface, compared to the bulk-like region, for both the LJ combination rules potential [21] and the parametrized Morse potential. The diffusion coefficients show that, in the interfacial region for both

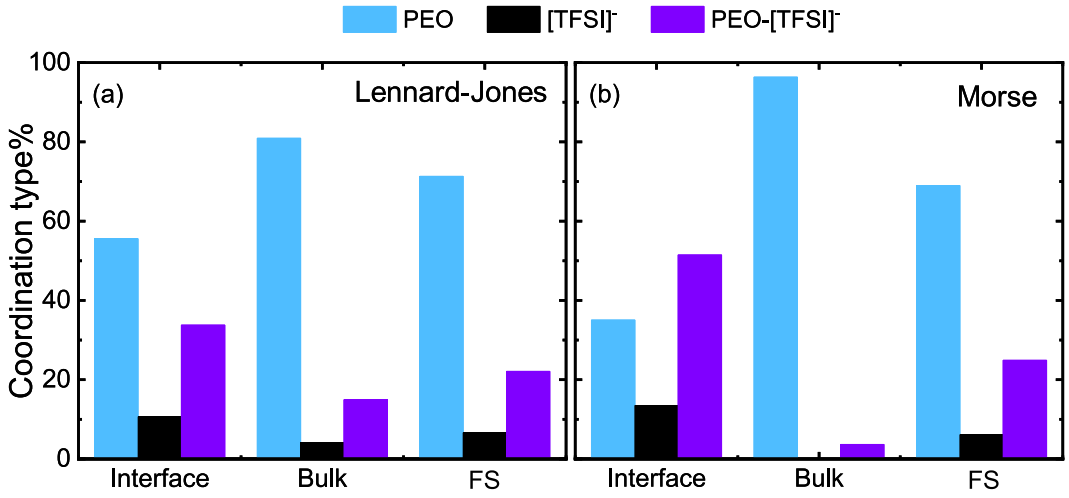


**Fig. 7.** Distribution of $[Li]^+$ coordination environments with PEO (blue), $[TFSI]^-$ (black), and PEO–$[TFSI]^-$ (purple) in different regions of the system: interface, bulk-like region, and full system (FS). (a) Lennard-Jones potential. (b) Morse potential.

models, $[Li]^+$ mobility is lower than that of the PEO chains, indicating that lithium transport is limited by its coordination to the polymer. Similarly, in the LJ bulk-like region, the diffusion coefficient of $[Li]^+$ is again lower than that of PEO. In contrast, in the Morse bulk-like region, $[Li]^+$ diffuses even faster than the polymer matrix, suggesting a decoupling from PEO and pointing to a distinct transport mechanism. The differences observed in the bulk-like region should therefore be interpreted as differences within the interfacial simulation, since the Li-metal surface may still influence this relatively small region, which cannot be considered an independent bulk-electrolyte system.

The diffusion coefficients obtained with the Morse potential are higher than the experimentally reported values [64]. This difference may be related to the different electrolyte-Li interaction profiles resulting from the DFT-based parameterization and the associated interfacial dynamics. Therefore, the comparison between the two interaction models is primarily focused on relative dynamical trends rather than on reproducing absolute experimental diffusion coefficients. Within this context, the Morse model yields the same qualitative ordering of the ionic diffusion coefficients observed experimentally, with ($D_{Li^+} < D_{TFSI^-}$) in both the bulk-like and interface regions.

### 4.3. Lithium mobility

To investigate the influence of the coordination environment on $[Li]^+$ mobility, we analyzed the van Hove correlation function, focusing on both the self part, $G_s(r,t)$, which describes the probability of finding a given particle at a distance r from its initial position after a time $t$, and the distinct part, $G_d(r,t)$, which characterizes the spatial correlation between different particles over a time interval. These functions are defined as:

$$G_s(\boldsymbol{r},t) = \frac{1}{N}\sum_{i=1}^{N}\left\langle \delta\left(r - |\boldsymbol{r}_i(t) - \boldsymbol{r}_i(0)|\right)\right\rangle, \quad (4)$$

$$G_d(\boldsymbol{r},t) = \frac{1}{N}\sum_{i=1}^{N}\sum_{j\neq i}^{N}\left\langle \delta\left(r - |\boldsymbol{r}_i(t) - \boldsymbol{r}_j(0)|\right)\right\rangle. \quad (5)$$

Fig. 8 shows the results for the function $4\pi r^2 G_s(r,t)$, which represents the probability of finding an ion at a distance $r$ from its initial position at $t = 0$. For $[Li]^+$ in the LJ model [ Fig. 8(a)], we observe that at short times (5–40 ns), the function displays a well-defined and centered peak that gradually shifts to larger $r$, indicating diffusive motion. At longer times, a second peak emerges, suggesting a combination of diffusive behavior and dynamic heterogeneity.

In contrast, the results in Fig. 8(b), corresponding to the Morse potential, show a well-defined single peak at 5 ns, consistent with diffusive motion. However, by 10 ns, the peak begins to show subtle distortions compared to the LJ case, indicating the emergence of dynamic heterogeneity. At longer times, multiple distinct and persistent peaks clearly emerge. By comparing the self-part of the van Hove function for $[Li]^+$ in the two models, it is evident that the peak in the Morse model is shifted to larger $r$ values compared to the LJ model. This indicates that $[Li]^+$ ions move farther from their initial positions in the same time interval, reflecting higher mobility in the Morse system.

To further characterize the local coordination environment associated with the heterogeneous dynamics observed in the self-part analysis, we next examine the distinct part of the van Hove correlation function, $G_d(r,t)$, for $[Li]^+$–$O_{TFSI}$ and $[Li]^+$–$O_{PEO}$ interactions at different time intervals, as shown in Fig. 9. In the case of $[Li]^+$–$O_{TFSI}$ [ Figs. 9(a) and (b)], a primary peak is observed at short times (1 ps) for both interaction potentials. However, this peak is broader and decays more rapidly in the system using the LJ potential, indicating a faster loss of self-correlation in the spatial distribution of ion pairs. In contrast, the Morse potential produces much sharper and more persistent peaks, particularly at short distances, reflecting a stronger and more stable local coordination environment. The presence of a secondary peak at larger distances in the distinct van Hove function indicates the existence of spatial correlations between different particles beyond the first coordination shell. This feature is often associated with second-neighbor interactions or extended local order.

In Figs. 9(c) and (d), the results for $[Li]^+$–$O_{PEO}$ show a similar overall behavior to the previous case. However, a notable feature is the presence of a distinct peak at $r = 0$ nm. This peak indicates a persistent spatial overlap between the same $[Li]^+$–$O_{PEO}$ pairs over time, suggesting that certain oxygen atoms within the PEO chains remain closely associated with specific lithium ions for extended durations. Such behavior reflects a trapped coordination environment.

Overall, the distinct van Hove analysis reveals that the Morse parameterization promotes a more structured local coordination environment, characterized by sharper coordination shells and longer-lived spatial correlations than the LJ model. Combined with the self-part analysis, these results show that the modified parameterization affects both the local structural organization and the lithium-ion dynamics.

To further examine whether the heterogeneous dynamics observed for $[Li]^+$ are also present in other components of the electrolyte, we analyzed the self-part of the van Hove correlation function for the $[TFSI]^-$ anion, focusing on the nitrogen atom located at the center of the molecule (Supplementary Material Figure S7). In the system

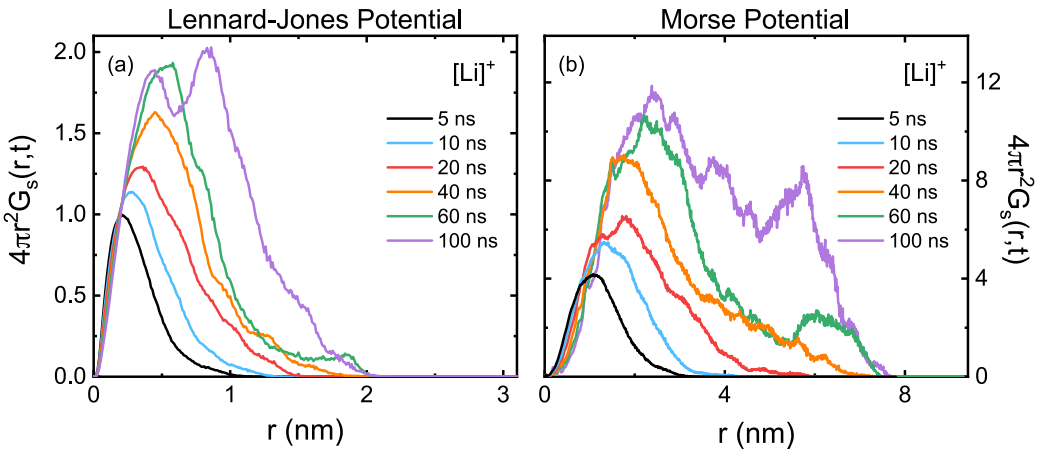


**Fig. 8.** Self-part of the van Hove correlation function, $G_s(r,t)$, for $[Li]^+$ ions computed at various time intervals for systems using (a) Lennard-Jones and (b) Morse interaction potentials.

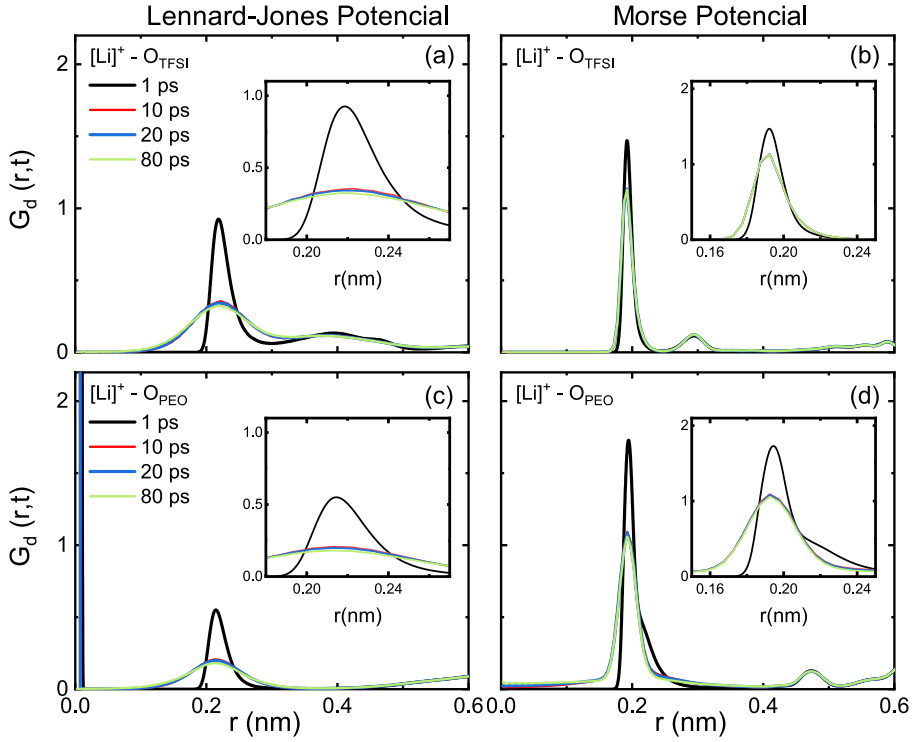


**Fig. 9.** The distinct part of van Hove function, $G_d(r,t)$, for $[Li]^+$-$O_{TFSI}$ (top) and $[Li]^+$-$O_{PEO}$ (bottom) computed at various time intervals for systems using (a,c) Lennard-Jones and (b,d) Morse interaction potentials.

described by the LJ potential, the main peak of $4\pi r^2 G_s(r,t)$ remains nearly stationary over time, indicating local confinement of the $N_{TFSI}$ atoms. Moreover, the appearance of secondary oscillations at longer times reflects a degree of dynamic heterogeneity, likely influenced by local structuring at the interface. In contrast, for the Morse potential [Figure S7(b)], the motion of $N_{TFSI}$ is predominantly diffusive at short times ($t < 5$ ns). As time progresses, however, the function becomes increasingly distorted and develops multiple peaks, suggesting a transition to heterogeneous dynamics.

To further interpret the heterogeneous dynamics and coordination effects discussed above, we performed a statistical classification of the transport mechanisms of $[Li]^+$ ions. Ion transport can be categorized, based on changes in the local coordination environment, into three main types: continuous, vehicular, and hopping [65]. In the continuous mechanism, the $[Li]^+$ ion diffuses while maintaining the same set of coordinating atoms over time, reflecting strong coupling with its local coordination shell. In the vehicular mechanism, the $[Li]^+$ ion is transported together with a larger coordination complex, such as a polymer segment, which migrates through the system. In contrast, the hopping mechanism involves discrete jumps of the $[Li]^+$ ion between different coordination environments, accompanied by rapid exchange of coordinating atoms. Following the methodology described in previous studies [65], each $[Li]^+$ trajectory was analyzed over a characteristic time interval of $\Delta t = 100$ ps to identify the dominant transport mechanism based on variations in the oxygen coordination environment and the total coordination number.

Fig. 10 shows the percentage of each transport mechanism of $[Li]^+$ ions for each coordinating species (PEO, $[TFSI]^-$, and mixed $[TFSI]^-$-PEO) in the full system, interface, and bulk-like regions for both model potentials. In general, we observe that the dominant microscopic transport mechanism for both models is vehicular, referring to the local ion–coordination dynamics rather than macroscopic polymer motion.

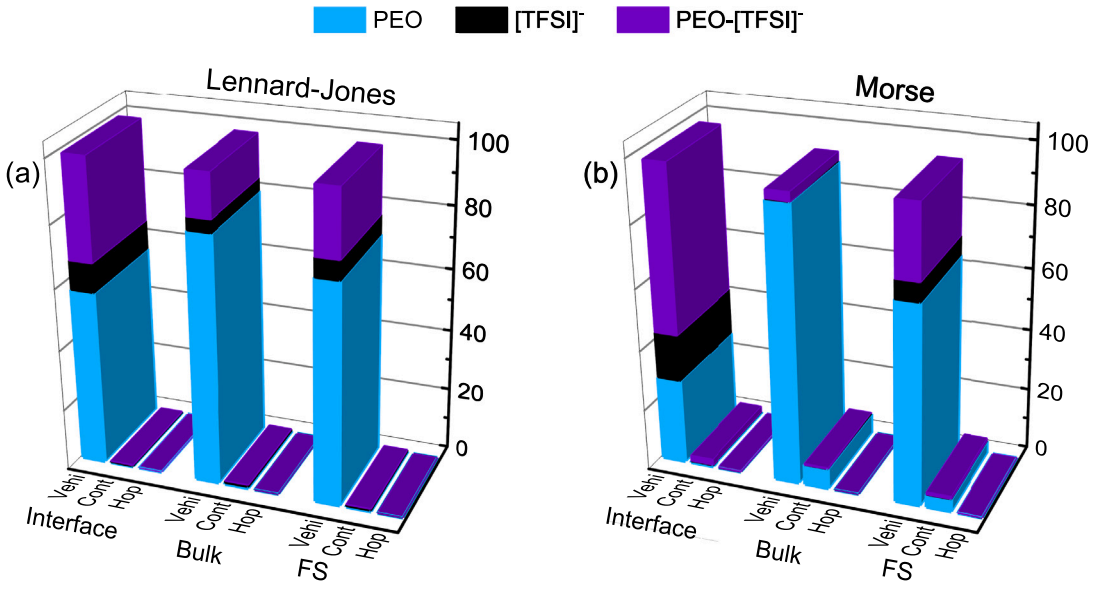


**Fig. 10.** Ion-transport mechanisms of $[Li]^+$ ions in interface, bulk-like region, and full system (FS), for two interaction models: (a) Lennard-Jones and (b) Morse. The color indicates the coordinating species: PEO (blue), $[TFSI]^-$ (black), and mixed PEO-$[TFSI]^-$ (purple).

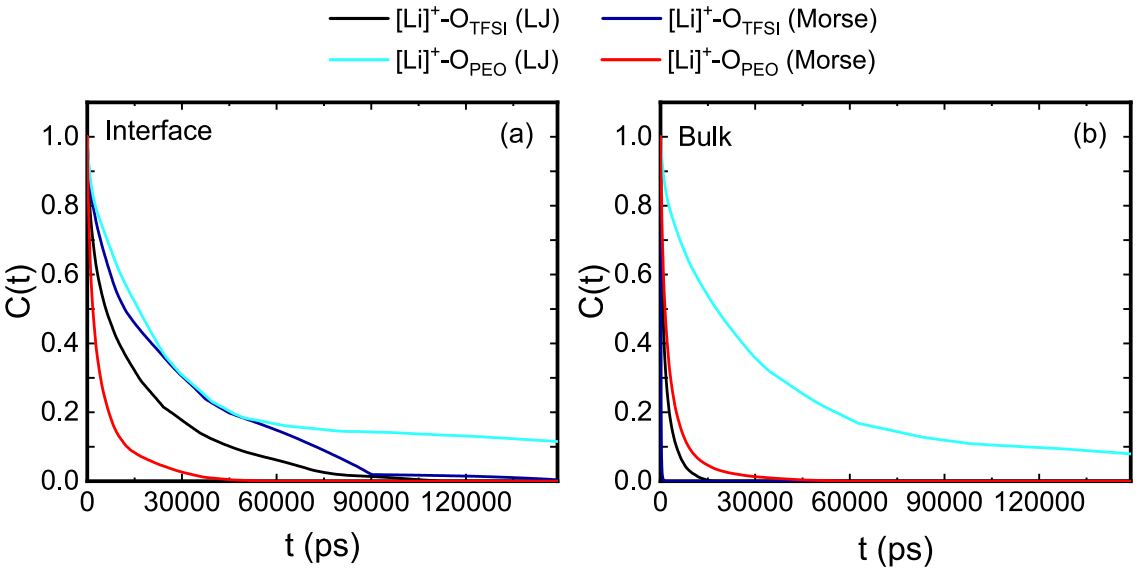


**Fig. 11.** Time correlation function, $C(t)$, for $[Li]^+$–$O_{TFSI}$ and $[Li]^+$–$O_{PEO}$ in the interface (left) and bulk-like region (right) regions for the Lennard-Jones and Morse interaction models.

This behavior is consistent with previous studies on PEO/LiTFSI polymer electrolytes, which showed that lithium transport in systems with short PEO chains is predominantly vehicular, with $[Li]^+$ ions moving together with the polymer segments, whereas systems with larger polymer molecular weight increasingly exhibit hopping transport between coordination sites [66]. However, at the interfaces, the LJ model [ Fig. 10(a)] shows most $[Li]^+$ ions being coordinated exclusively by PEO, while the Morse potential [ Fig. 10(b)] exhibits vehicular motion with a stronger contribution from $[TFSI]^-$-PEO coordinated ions. In the bulk-like region, the Morse potential model also shows a small contribution from the continuous mechanism. These results suggest that in the LJ system, vehicular transport involving PEO leads to more diffusive behavior over longer timescales. In contrast, the Morse model favors a mixed coordination environment involving both PEO and $[TFSI]^-$, which rapidly gives rise to dynamic heterogeneity.

The temporal stability of the coordination environments was further analyzed through the correlation function $C(t)$ for $[Li]^+$–$O_{PEO}$ and $[Li]^+$–$O_{TFSI}$ in both interface and bulk-like regions, as shown in Fig. 11. The correlation function is defined as

$$C(t) = \frac{\langle h(0)h(t)\rangle}{\langle h(0)\rangle}, \tag{6}$$

where $h(t) = 1$ if a given ion pair remains coordinated at time $t$, and $h(t) = 0$ otherwise. The coordination criterion for both $[Li]^+$–$O_{PEO}$ and $[Li]^+$–$O_{TFSI}$ pairs was defined based on the distance between the corresponding atoms, which must be less than or equal to the first minimum of the respective radial distribution function.

At the interface, the LJ model exhibits a markedly slower decay of the $[Li]^+$–$O_{PEO}$ correlation compared to the Morse model, indicating that $[Li]^+$ ions remain trapped within long-lived PEO coordination cages [ Fig. 11(a)]. A similar trend is observed in the bulk-like region [ Fig. 11(b)], where the LJ model exhibits a much slower decay of the $[Li]^+$–OPEO correlation than the Morse model, indicating more

**Table 2**
Interfacial and bulk-like region residence lifetimes ($\tau$) of $[Li]^+$ coordination pairs with $O_{PEO}$ and $O_{TFSI}$ for Morse and Lennard-Jones models.

| Coordination pair | Interfacial Region (ns) | | Bulk-like region (ns) | |
|---|---|---|---|---|
| | Morse | LJ | Morse | LJ |
| Li-$O_{PEO}$ | 5.16 | 431.15 | 3.71 | 60.24 |
| Li-$O_{TFSI}$ | 26.57 | 16.54 | – | 1.88 |

persistent coordination of $[Li]^+$ by the polymer. Together, these observations are consistent with the predominance of PEO-coordinated $[Li]^+$ populations (Fig. 7), the heterogeneous $[Li]^+$ density maps (Fig. 5), and the strongly reduced $[Li]^+$ mobility observed in Table 1. In contrast, the faster decay of the $[Li]^+$–OPEO correlation in the Morse model reflects a more frequent reorganization of the $[Li]^+$ solvation shell, involving both PEO and $[TFSI]^-$ oxygen atoms. The increased participation of $[TFSI]^-$ in the first coordination shell promotes mixed coordination environments and reduces the lifetime of purely polymer-coordinated $[Li]^+$ states. As a result, $[Li]^+$ ions experience a more dynamic solvation environment, leading to enhanced mobility and a more homogeneous spatial distribution throughout the system. These effects are a consequence of the modified electrolyte–metal interactions introduced by the parametrized Morse potential, which promote interfacial enrichment of ionic species and consequently alter the local coordination structure of $[Li]^+$.

Previous studies on PEO-based polymer electrolytes have combined neutron scattering experiments, dielectric spectroscopy, and molecular dynamics simulations to investigate the microscopic mechanism of $[Li]^+$ transport [67]. These works have provided direct evidence that $[Li]^+$ ions are transiently coordinated by ether oxygen atoms of the polymer, forming well-defined coordination cages. By analyzing time-resolved scattering functions and ion–oxygen coordination statistics, these studies were able to estimate characteristic residence (cage) times on the order of a few nanoseconds (~4–7 ns), depending on temperature and composition. In the present work, we computed the $[Li]^+$ lifetimes associated with these coordination environments, which are reported in Table 2. The values were determined from a biexponential fit of the correlation function, $C(t)$. The results indicate that the Morse potential yields nanosecond-scale values consistent with the dynamic cage picture reported in the literature [67], whereas the LJ description systematically overestimates $[Li]^+$ confinement, particularly at the interface, leading to artificially long residence times.

## 5. Conclusion

In this work, we investigated the structural and dynamical properties of PEO/LiTFSI polymer electrolytes in contact with lithium metal using two different descriptions for the electrolyte–metal interactions: a standard Lennard-Jones model based on geometric combination rules and a specifically parametrized Morse potential derived from interaction energy calculations. The results demonstrate that the choice of interaction potential has a significant impact on the predicted interfacial organization, local coordination environment, and lithium transport mechanisms.

The parametrized Morse potential promotes a stronger accumulation of $[Li]^+$ and $[TFSI]^-$ ions near the lithium metal surface, leading to an interfacial region enriched in ionic species. In contrast, the Lennard-Jones model favors a more polymer-rich interfacial structure. The structural analyses based on density profiles, coordination statistics, and radial distribution functions further show that the Morse potential enhances the participation of $[TFSI]^-$ in the $[Li]^+$ coordination shell at the interface, producing a mixed PEO–$[TFSI]^-$ coordination environment.

These structural differences strongly affect the transport properties of the electrolyte. The parametrized Morse model yields higher self-diffusion coefficients for all species and produces a more homogeneous spatial distribution of $[Li]^+$ ions throughout the system. In contrast, the Lennard-Jones model exhibits more persistent $[Li]^+$–PEO correlations and localized Li-rich regions. The analysis of the transport mechanisms further reveals that lithium transport is predominantly vehicular in both systems, consistent with previous studies on short-chain PEO electrolytes. However, the Morse model exhibits stronger dynamic heterogeneity and enhanced contributions from mixed PEO–$[TFSI]^-$ coordination, suggesting a more dynamic and less polymer-confined lithium transport mechanism.

Overall, the results indicate that the parametrized Morse potential provides a substantially different microscopic description of the lithium metal–polymer electrolyte interface compared to the conventional Lennard-Jones approach. In particular, the stronger ionic accumulation and enhanced participation of $[TFSI]^-$ near the metallic surface predicted by the Morse model appear more consistent with experimentally proposed lithium-rich interfacial environments in PEO/LiTFSI systems. These findings highlight the importance of accurately describing metal–electrolyte interactions in atomistic simulations of solid polymer electrolytes and demonstrate that the choice of interaction potential can strongly influence the predicted interfacial structure and ion transport behavior.

This model may provide a basis for future studies of other polymer-based solid-state battery systems. However, its broader applicability to systems with different polymer chemistries, electrolyte compositions, and electrode materials would require further validation. Such studies should include system-specific parameterization based on DFT calculations, together with comparison with available experimental data and rigorous higher-level computational results. The transferability of the approach should also be examined by evaluating structural, dynamical, and thermodynamic properties across different systems. In addition, the effects of electrode polarization, charge transfer, and interfacial chemical reactions should be considered when extending the model to realistic electrochemical interfaces and SEI formation. These studies would help establish the transferability and limitations of the proposed approach beyond the Li/PEO-LiTFSI interface investigated here.

## CRediT authorship contribution statement

**Vanessa Torres:** Writing – review & editing, Writing – original draft, Visualization, Methodology, Investigation, Formal analysis. **Mahsa Ebadi:** Writing – review & editing, Validation, Methodology, Formal analysis, Conceptualization. **Tuanan C. Lourenço:** Writing – review & editing, Visualization, Formal analysis, Conceptualization. **Marcelo Albuquerque:** Writing – review & editing, Visualization, Methodology, Investigation, Conceptualization. **Pedro Venezuela:** Writing – review & editing, Visualization, Supervision. **Luana S. Pedroza:** Writing – review & editing, Visualization. **C. Moyses Araujo:** Writing – review & editing, Visualization. **Daniel Brandell:** Writing – review & editing, Visualization, Formal analysis, Conceptualization. **Luciano T. Costa:** Writing – review & editing, Visualization, Supervision, Project administration, Investigation, Formal analysis, Conceptualization.

## Declaration of competing interest

The authors declare that they have no known competing financial interests or personal relationships that could have appeared to influence the work reported in this paper.

## Acknowledgments

We thank the Brazilian funding agencies FAPERJ, CAPES, and CNPq for their financial support. V. T. thanks CNPq (Grant No. 351283/2023-4) and CNPq INCT Materials Informatics project (number 406447/2022-5 Grant No 150163/2026-6). M. A. acknowledges the CNPq Knowledge Brazil project (Grant No. 447482/2024-6) and the CNPq INCT Materials

Informatics project (number 406447/2022-5) for their financial support, as well as the CAPES/STINT project (number 88887.660802/2021-00). L.T.C. thanks the CNPq fellowship (grant number 306032/2019-8), the research program FAPERJ/APQ-1 (grant number E-26/210.376/2019), the CAPES/PRINT project (grant number 88881.310460/2018-01) and CNPq/MCTI 44/2024 – Processo: 409108/2025-1 e 307572/2022-6 (CNPq Fellowship).

Support for Joint Brazilian-Sweden Research Collaboration from CAPES/STINT is gratefully acknowledged. This project was supported by the Swedish Energy Agency grant number 39036-1 and STandUP for Energy. The computations were carried out on resources provided by the National Academic Infrastructure for Supercomputing in Sweden (NAISS) at the NSC and PDC Center for High Performance Computing.

## Appendix A. Supplementary data

This supplementary material includes files with additional data that support and complement the findings presented in the manuscript, providing further insights and supporting analyses. The ff.rar file provides the force field parameters used in the simulations, along with other relevant input files. The files are also available on the following website: https://github.com/molmodcs/Li-metal-anode-simulations

Supplementary material related to this article can be found online at https://doi.org/10.1016/j.electacta.2026.150036.

## Data availability

The data and code supporting the findings of this study are openly available at https://github.com/molmodcs/Li-metal-anode-simulations.

## References

[1] L. Fan, S. Wei, S. Li, Q. Li, Y. Lu, Recent progress of the solid-state electrolytes for high-energy metal-based batteries, Adv. Energy Mater. 8 (11) (2018) 1702657.
[2] P. Nzereogu, A. Oyesanya, S. Ogba, S. Ayanwunmi, M. Sobajo, V. Chimsunum, V. Ayanwunmi, M. Amoo, O. Adefemi, C. Chukwudi, Solid-state lithium-ion battery electrolytes: Revolutionizing energy density and safety, Hybrid Adv. 8 (2025) 100339.
[3] X.-B. Cheng, R. Zhang, C.-Z. Zhao, F. Wei, J.-G. Zhang, Q. Zhang, A review of solid electrolyte interphases on lithium metal anode, Adv. Sci. 3 (3) (2016) 1500213.
[4] S.F. Mayer, B. Mercier-Guyon, C. Doublet, A. Fauchier-Magnan, L.R. Mangani, C. Renais, M. Reuter, O. Thompson, L. Trassart, C. Villevieille, Understanding interphases and interfaces of battery materials at the nanoscale, Small 21 (2025) 2504379.
[5] H. Li, Z. Ao, Y. Wan, Y. Liang, P. Li, Y. Zou, PEO kaolinite intercalation interface accelerates lithium-ion transfer for all-solid-state lithium metal batteries, Electrochim. Acta 507 (2024) 145011.
[6] Y. Zhu, W. Bai, B. Lu, J. Ma, S. Chen, H. Wang, B. Liu, S. Xiong, Z. Song, X. Wang, et al., Electrochemical behavior of lithium metal anodes in solid polymer electrolytes: The impact of current density and capacity, Electrochim. Acta (2026) 148923.
[7] W. Li, T. Sun, S.R. Shah, Z. Ju, J. Zhou, K. Zhao, G. Yu, Y. Liu, Direct optical observation of solid electrolyte interphase formation dynamics in lithium-ion batteries, Proc. Natl. Acad. Sci. 123 (10) (2026) e2531794123.
[8] C. Sångeland, J. Mindemark, R. Younesi, D. Brandell, Probing the interfacial chemistry of solid-state lithium batteries, Solid State Ion. 343 (2019) 115068.
[9] K. Johnston, V. Harmandaris, Hierarchical simulations of hybrid polymer–solid materials, Soft Matter 9 (29) (2013) 6696–6710.
[10] J. Zhang, M.B. Sullivan, J.W. Zheng, K.P. Loh, P. Wu, Theoretical study on polyimide- cu (100)/Ni (100) adhesion, Chem. Mater. 18 (22) (2006) 5312–5316.
[11] T. Semoto, Y. Tsuji, K. Yoshizawa, Molecular understanding of the adhesive force between a metal oxide surface and an epoxy resin, J. Phys. Chem. C 115 (23) (2011) 11701–11708.
[12] V.A. Harmandaris, K.C. Daoulas, V.G. Mavrantzas, Molecular dynamics simulation of a polymer melt/solid interface: Local dynamics and chain mobility in a thin film of polyethylene melt adsorbed on graphite, Macromolecules 38 (13) (2005) 5796–5809.
[13] A.N. Rissanou, V. Harmandaris, Structural and dynamical properties of polystyrene thin films supported by multiple graphene layers, Macromolecules 48 (8) (2015) 2761–2772.
[14] A. Rivera-Pousa, J.M. Otero-Mato, H. Montes-Campos, T. Méndez-Morales, D. Diddens, A. Heuer, L.M. Varela, Ternary solid polymer electrolytes at the electrochemical interface: A computational study, Macromolecules 57 (9) (2024) 3921–3936.
[15] W.L. Jorgensen, D.S. Maxwell, J. Tirado-Rives, Development and testing of the OPLS all-atom force field on conformational energetics and properties of organic liquids, J. Am. Chem. Soc. 118 (45) (1996) 11225–11236.
[16] M. Ebadi, C. Marchiori, J. Mindemark, D. Brandell, C.M. Araujo, Assessing structure and stability of polymer/lithium-metal interfaces from first-principles calculations, J. Mater. Chem. A 7 (14) (2019) 8394–8404.
[17] T.C. Lourenço, M. Ebadi, D. Brandell, J.L. Da Silva, L.T. Costa, Interfacial structures in ionic liquid-based ternary electrolytes for lithium-metal batteries: a molecular dynamics study, J. Phys. Chem. B 124 (43) (2020) 9648–9657.
[18] A. Thum, D. Diddens, A. Heuer, Impact of charged surfaces on the structure and dynamics of polymer electrolytes: Insights from atomistic simulations, J. Phys. Chem. C 125 (46) (2021) 25392–25403.
[19] Ø. Gullbrekken, F. Bresme, S. Selbach, S. Schnell, Electric double layer studies of li electrode—PEO-litfsi electrolyte by constant potential simulations, J. Chem. Phys. 164 (7) (2026) 074708.
[20] L.-T. Wu, Y.-T. Zhan, B.J. Hwang, D. Brandell, J.-C. Jiang, Understanding the role of residual water in poly (ethylene oxide)-based electrolytes at the anode interface through atomistic modeling, J. Energy Storage 152 (2026) 120727.
[21] M. Ebadi, L.T. Costa, C.M. Araujo, D. Brandell, Modelling the polymer electrolyte/li-metal interface by molecular dynamics simulations, Electrochim. Acta 234 (2017) 43–51.
[22] A. Berg, C. Peter, K. Johnston, Evaluation and optimization of interface force fields for water on gold surfaces, J. Chem. Theory Comput. 13 (11) (2017) 5610–5623.
[23] L.R. Safina, E.A. Rozhnova, R.T. Murzaev, J.A. Baimova, Effect of interatomic potential on simulation of fracture behavior of cu/graphene composite: A molecular dynamics study, Appl. Sci. 13 (2) (2023) 916.
[24] P. Kang, D. Chen, L. Wu, X. Yang, G. Sui, Insight into poly (1, 3-dioxolane)-based polymer electrolytes and their interfaces with lithium metal: Effect of electrolyte compositions, Chem. Eng. J. 455 (2023) 140931.
[25] J.N. Canongia Lopes, A.A. Pádua, Molecular force field for ionic liquids composed of triflate or bistriflylimide anions, J. Phys. Chem. B 108 (43) (2004) 16893–16898.
[26] H. Gudla, C. Zhang, D. Brandell, Effects of solvent polarity on li-ion diffusion in polymer electrolytes: An all-atom molecular dynamics study with charge scaling, J. Phys. Chem. B 124 (37) (2020) 8124.
[27] V. Ganesan, Z. Zhang, N. Marioni, Dynamical ion correlations in polymer and membrane electrolytes: Recent advances and open questions, J. Phys. Chem. Lett. 16 (32) (2025) 8114–8124.
[28] Y. Shao, H. Gudla, J. Mindemark, D. Brandell, C. Zhang, Ion transport in polymer electrolytes: Building new bridges between experiment and molecular simulation, Acc. Chem. Res. 57 (8) (2024) 1123.
[29] L.T. Costa, B. Sun, F. Jeschull, D. Brandell, Polymer-ionic liquid ternary systems for li-battery electrolytes: Molecular dynamics studies of LiTFSI in a EMIm-TFSI and PEO blend, J. Chem. Phys. 143 (2) (2015) 024904.
[30] N. Molinari, J.P. Mailoa, B. Kozinsky, Effect of salt concentration on ion clustering and transport in polymer solid electrolytes: a molecular dynamics study of PEO–litfsi, Chem. Mater. 30 (18) (2018) 6298–6306.
[31] M.J. Frisch, G.W. Trucks, H.B. Schlegel, G.E. Scuseria, M.A. Robb, J. Cheeseman, V. Scalmani, G.A. Petersson, X. Nakatsuji, M. Caricato, A.V. Marenich, J. Bloino, B.G. Janesko, R. Gomperts, B. Mennucci, D.J. Hratch, Gaussian 16, revision b.01. Gaussian, inc.: Wallingford CT, 2016.
[32] Y. Zhao, D.G. Truhlar, The M06 suite of density functionals for main group thermochemistry, thermochemical kinetics, noncovalent interactions, excited states, and transition elements: two new functionals and systematic testing of four M06-class functionals and 12 other functionals, Theor. Chem. Accounts 120 (1) (2008) 215–241.
[33] Y. Zhao, D.G. Truhlar, Density functional theory for reaction energies: test of meta and hybrid meta functionals, range-separated functionals, and other high-performance functionals, J. Chem. Theory Comput. 7 (3) (2011) 669–676.
[34] R. Ditchfield, W.J. Hehre, J.A. Pople, Self-consistent molecular-orbital methods. IX. An extended Gaussian-type basis for molecular-orbital studies of organic molecules, J. Chem. Phys. 54 (2) (1971) 724–728.
[35] T.H. Dunning Jr., Gaussian basis sets for use in correlated molecular calculations. I. the atoms boron through neon and hydrogen, J. Chem. Phys. 90 (2) (1989) 1007–1023.
[36] A. Schäfer, H. Horn, R. Ahlrichs, Fully optimized contracted Gaussian basis sets for atoms Li to Kr, J. Chem. Phys. 97 (4) (1992) 2571–2577.
[37] A. Schäfer, C. Huber, R. Ahlrichs, Fully optimized contracted Gaussian basis sets of triple zeta valence quality for atoms Li to Kr, J. Chem. Phys. 100 (8) (1994) 5829–5835.
[38] S.F. Boys, F. Bernardi, The calculation of small molecular interactions by the differences of separate total energies. Some procedures with reduced errors, Mol. Phys. 19 (4) (1970) 553–566.
[39] D. Roest, P. Ballone, D. Bedeaux, S. Kjelstrup, Molecular dynamics simulations of metal/molten alkali carbonate interfaces, J. Phys. Chem. C 121 (33) (2017) 17827–17847.

[40] L.-T. Kong, C. Denniston, M.H. Müser, Y. Qi, Non-bonded force field for the interaction between metals and organic molecules: a case study of olefins on aluminum, Phys. Chem. Chem. Phys. 11 (43) (2009) 10195–10203.
[41] K. Johnston, V. Harmandaris, Properties of benzene confined between two Au (111) surfaces using a combined density functional theory and classical molecular dynamics approach, J. Phys. Chem. C 115 (30) (2011) 14707–14717.
[42] L. Yang, L. Sun, W.-Q. Deng, Combination rules for morse-based van der waals force fields, J. Phys. Chem. A 122 (6) (2018) 1672–1677.
[43] S. Kwon, H.J. Kwon, J.I. Choi, K.C. Kim, J.G. Seo, J.E. Park, S.J. You, E.D. Park, S.S. Jang, H.C. Lee, Enhanced selectivity for CO2 adsorption on mesoporous silica with alkali metal halide due to electrostatic field: A molecular simulation approach, ACS Appl. Mater. Interfaces 9 (37) (2017) 31683–31690.
[44] A.C. Mendonça, P. Malfreyt, A.A. Pádua, Interactions and ordering of ionic liquids at a metal surface, J. Chem. Theory Comput. 8 (9) (2012) 3348–3355.
[45] M. Jäckle, A. Groß, Microscopic properties of lithium, sodium, and magnesium battery anode materials related to possible dendrite growth, J. Chem. Phys. 141 (17) (2014) 174710.
[46] L.-T. Wu, E.K. Andersson, M. Hahlin, J. Mindemark, D. Brandell, J.-C. Jiang, A method for modelling polymer electrolyte decomposition during the Li-nucleation process in Li-metal batteries, Sci. Rep. 13 (1) (2023) 9060.
[47] E.K. Andersson, C. Sångeland, E. Berggren, F.O. Johansson, D. Kühn, A. Lindblad, J. Mindemark, M. Hahlin, Early-stage decomposition of solid polymer electrolytes in Li-metal batteries, J. Mater. Chem. A 9 (39) (2021) 22462–22471.
[48] E.K. Andersson, L.-T. Wu, L. Bertoli, Y.-C. Weng, D. Friesen, K. Elbouazzaoui, S. Bloch, R. Ovsyannikov, E. Giangrisostomi, D. Brandell, et al., Initial SEI formation in LiBOB-, LiDFOB-and LiBF 4-containing PEO electrolytes, J. Mater. Chem. A 12 (15) (2024) 9184–9199.
[49] M.J. Abraham, T. Murtola, R. Schulz, S. Páll, J.C. Smith, B. Hess, E. Lindahl, GROMACS: High performance molecular simulations through multi-level parallelism from laptops to supercomputers, SoftwareX 1–2 (2015) 19–25.
[50] B. Hess, C. Kutzner, D. Van Der Spoel, E. Lindahl, GROMACS 4: algorithms for highly efficient, load-balanced, and scalable molecular simulation, J. Chem. Theory Comput. 4 (3) (2008) 435–447.
[51] L. Martínez, R. Andrade, E.G. Birgin, J.M. Martínez, PACKMOL: A package for building initial configurations for molecular dynamics simulations, J. Comput. Chem. 30 (13) (2009) 2157–2164.
[52] G. Bussi, D. Donadio, M. Parrinello, Canonical sampling through velocity rescaling, J. Chem. Phys. 126 (1) (2007) 014101.
[53] T. Darden, D. York, L. Pedersen, Particle mesh Ewald: An N log (N) method for Ewald sums in large systems, J. Chem. Phys. 98 (12) (1993) 10089–10092.
[54] G.B. Damas, A.B. Dias, L.T. Costa, A quantum chemistry study for ionic liquids applied to gas capture and separation, J. Phys. Chem. B 118 (30) (2014) 9046–9064.
[55] Y. Zhang, E.J. Maginn, A simple AIMD approach to derive atomic charges for condensed phase simulation of ionic liquids, J. Phys. Chem. B 116 (33) (2012) 10036–10048.
[56] C. Schröder, Comparing reduced partial charge models with polarizable simulations of ionic liquids, Phys. Chem. Chem. Phys. 14 (9) (2012) 3089–3102.
[57] J. Wang, R.M. Wolf, J.W. Caldwell, P.A. Kollman, D.A. Case, Development and testing of a general amber force field, J. Comput. Chem. 25 (9) (2004) 1157–1174.
[58] W. Xu, J. Wang, F. Ding, X. Chen, E. Nasybulin, Y. Zhang, J.-G. Zhang, Lithium metal anodes for rechargeable batteries, Energy Environ. Sci. 7 (2) (2014) 513–537.
[59] C. Xu, B. Sun, T. Gustafsson, K. Edström, D. Brandell, M. Hahlin, Interface layer formation in solid polymer electrolyte lithium batteries: an XPS study, J. Mater. Chem. A 2 (20) (2014) 7256–7264.
[60] T. Weintraut, A. Weiss, S.L. Benz, B. Aktekin, J. Sann, A. Henss, Unveiling SEI formation dynamics of PEO: LiTFSI with lithium metal: An in situ approach combining SIMS, XPS, and CTTA, Adv. Mater. Interfaces 12 (23) (2025) e00392.
[61] B.A. Fortuin, J. Otegi, J.M.L. Del Amo, S.R. Peña, L. Meabe, H. Manzano, M. Martínez-Ibañez, J. Carrasco, Synergistic theoretical and experimental study on the ion dynamics of bis (trifluoromethanesulfonyl) imide-based alkali metal salts for solid polymer electrolytes, Phys. Chem. Chem. Phys. 25 (36) (2023) 25038–25054.
[62] H. Gudla, Y. Shao, S. Phunnarungsi, D. Brandell, C. Zhang, Importance of the ion-pair lifetime in polymer electrolytes, J. Phys. Chem. Lett. 12 (35) (2021) 8460–8464.
[63] D. Sharon, P. Bennington, M.A. Webb, C. Deng, J.J. De Pablo, S.N. Patel, P.F. Nealey, Molecular level differences in ionic solvation and transport behavior in ethylene oxide-based homopolymer and block copolymer electrolytes, J. Am. Chem. Soc. 143 (8) (2021) 3180–3190.
[64] D.M. Pesko, K. Timachova, R. Bhattacharya, M.C. Smith, I. Villaluenga, J. Newman, N.P. Balsara, Negative transference numbers in poly (ethylene oxide)-based electrolytes, J. Electrochem. Soc. 164 (11) (2017) E3569–E3575.
[65] H. Gudla, A. Hockmann, D. Brandell, J. Mindemark, To hop or not to hop: Unveiling different modes of ion transport in solid polymer electrolytes through molecular dynamics simulations, ACS Appl. Polym. Mater. 7 (8) (2025) 4716–4724.
[66] D. Devaux, R. Bouchet, D. Glé, R. Denoyel, Mechanism of ion transport in PEO/LiTFSI complexes: Effect of temperature, molecular weight and end groups, Solid State Ion. 227 (2012) 119–127.
[67] C. Do, P. Lunkenheimer, D. Diddens, M. Götz, M. Weiß, A. Loidl, X.-G. Sun, J. Allgaier, M. Ohl, Li+ transport in poly (Ethylene Oxide) based electrolytes: Neutron scattering, dielectric spectroscopy, and molecular dynamics simulations, Phys. Rev. Lett. 111 (1) (2013) 018301.